Spin ordering and orbital ordering transitions in MnV_2O_4

H. D. Zhou,[1,2] J. Lu,[2] and C. R. Wiebe[1,2,*]

[1]*Department of Physics, Florida State University, Tallahassee, Florida 32306-3016, USA*

[2]*National High Magnetic Field Laboratory, Florida State University, Tallahassee, Florida 32306-4005, USA*

(Received 11 June 2007; revised manuscript received 6 August 2007; published 2 November 2007)

We present low-temperature x-ray diffraction, susceptibility, specific heat, and thermal conductivity results both on single crystal and polycrystalline MnV_2O_4. The single crystal sample exhibits two transitions: a spin ordering (ferrimagnetic) transition at $T_{SO}=56$ K and an orbital ordering transition at $T_{OO}=52$ K. The structural change and phase separation at T_{OO} suggest that the transition is first order. With applied magnetic fields, both T_{SO} and T_{OO} increase and T_{OO} disappears with $H \geqslant 0.5$ T. The polycrystalline sample just exhibits one transition at 55 K. The difference between the single crystal and polycrystalline samples is due to the nonstoichiometric polycrystalline sample.

DOI: 10.1103/PhysRevB.76.174403 PACS number(s): 75.50.Gg, 61.10.Nz, 65.40.Ba, 66.70.+f

I. INTRODUCTION

Cubic spinels AB_2O_4 with magnetic B ions have attracted considerable attention recently in light of geometrical frustration intrinsic to the B-site sublattice of corner-sharing tetrahedra.[1] When the B site is occupied by the V^{3+} ion, which takes the $3d^2$ high-spin configuration in the triply degenerate t_{2g} orbital, and has orbital degrees of freedom, complex electronic and magnetic properties emerge. The oxides AV_2O_4 [with divalent ions such as A=Zn,[2] Mg,[3] and Cd (Ref. 4)] are Mott insulators that undergo two separate phase transitions at low temperatures, usually a structural transition followed by a magnetic transition. Recent neutron scattering data on ZnV_2O_4 has confirmed that this structural phase transition to a tetragonal symmetry can be regarded as an orbital ordering of V ions along [110] chains.[2] Different models have been proposed for this orbital ordering, either based on the Kugel-Khomskii-type coupling on the V site[5] or spin-orbit coupling and cooperative Jahn-Teller coupling.[6] However, there are few reports in the literature on the control of the orbital state by an applied magnetic field in these t_{2g} systems. The main problem is that most of the t_{2g} systems have dominant antiferromagnetic interactions and, thus, are not sensitive to the applied magnetic fields. On the other hand, the orbital-spin coupling for e_g systems is a popular topic. For example, in hole doped perovskite manganites, in which doubly degenerate e_g orbitals of the Mn $3d$ state are occupied by one electron, applied magnetic fields align the Mn spins in the same direction. The Mn orbital state changes, resulting in "colossal magnetoresistance."[7]

MnV_2O_4 is a spinel which has additional magnetic Mn^{2+} ions ($3d^5$ high-spin configuration with no orbital degrees of freedom) in the crystal lattice to enhance the effect of the magnetic field. Plumier and Saugi[8,9] first reported that there is a ferromagnetic transition at 56 K and a structural transition from cubic to tetragonal phase around 53 K for MnV_2O_4 by neutron diffraction experiments. Recently, Katsufuji and co-workers[10,11] reported a magnetic field "switching" of the crystal structure in MnV_2O_4. It was demonstrated that the applied magnetic field enhances the evolution of a ferromagnetic moment on the V site and thus induces an orbital ordering and the structural phase transition into a tetragonal phase. However, they also reported that there is only one transition temperature at 57 K with the magnetic and structural transitions occurring simultaneously for single crystals (although their other publication[11] on a polycrystalline sample claimed that there are two transitions). Therefore, the controversy is whether there are one or two transitions at low temperatures for MnV_2O_4, which seems to be an issue of sample quality. If there are two transitions with the magnetic transition occurring before the structural transition, this makes MnV_2O_4 unique and different from other AV_2O_4 compounds mentioned above, in which magnetic ordering only can occur after the structural transition. Surprisingly, besides the references mentioned above, no other experiments have been reported to clarify this issue.

Here, we present detailed structural, magnetic, specific heat, and thermal conductivity data both on single crystal (SC) and polycrystalline (PC) MnV_2O_4. The SC exhibits two transitions: a spin ordering transition at $T_{SO}=56$ K and an orbital ordering transition with a structural distortion at $T_{OO}=52$ K. The PC just exhibits one transition at 55 K. The reason for this difference is discussed.

II. EXPERIMENT

PC MnV_2O_4 was made by solid state reaction. Stoichiometric mixture of MnO and V_2O_3 were ground together and calcined in vacuum in a sealed quartz tube at 950 °C for 40 h. A SC of MnV_2O_4 was grown by the traveling-solvent floating-zone technique. The feed and seed rods for the crystal growth were prepared by solid state reaction. Appropriate mixtures of MnO and V_2O_3 were ground together and pressed into 6-mm-diameter 60 mm rods under 400 atm hydrostatic pressure, and then calcined in vacuum in a sealed quartz tube at 950 °C for 12 h. The crystal growth was carried out in argon in an IR-heated image furnace (NEC) equipped with two halogen lamps and double ellipsoidal mirrors with feed and seed rods rotating in opposite directions at 25 rpm during crystal growth at a rate of 30 mm/h. Due to the evaporation of V_2O_3 during the growth, extra V_2O_3 in the starting material and high growth speeds are critical to

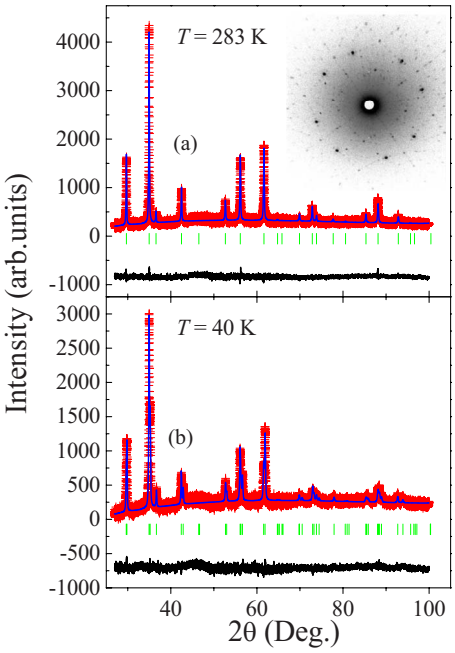

FIG. 1. (Color online) XRD patterns (plus marks) for SC at (a) 283 K and (b) 40 K. The solid curves are the best fits from the Rietveld refinement using FULLPROF. The vertical marks indicate the position of Bragg peaks and the bottom curves show the difference between the observed and calculated intensities. Inset of (a), Laue back diffraction pattern for crystal oriented along the [100] axis.

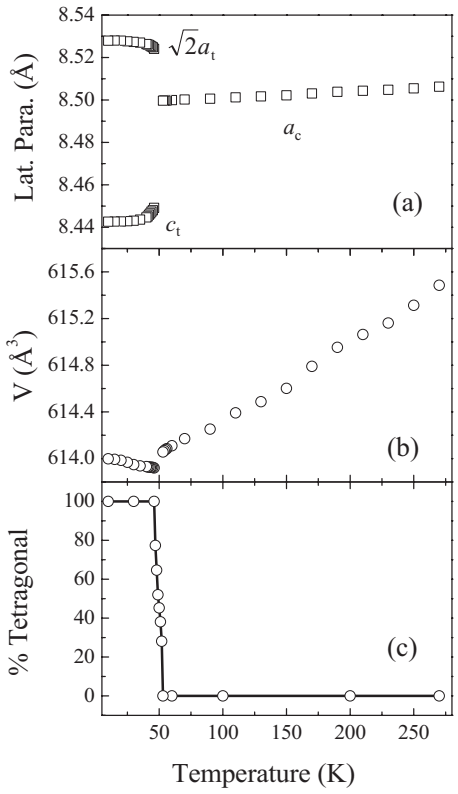

FIG. 2. Temperature dependencies of the (a) lattice parameters, (b) volume, and (c) phase fraction of the low-temperature tetragonal phase for SC MnV_2O_4.

obtain high quality samples. Small pieces of SC were groundinto fine powder for x-ray diffraction (XRD). The XRD patterns were recorded by a HUBER Imaging Plate Guinier Camera 670 with Cu $K\alpha_1$ radiation (1.540 59 Å) with a Ge monochromator. Data were collected in steps of 0.005° over the range $26° \leqslant 2\theta \leqslant 100°$ with temperatures down to 10 K obtained by a cryogenics with He compressor. XRD data were fitted from the Rietveld refinement by using the FULLPROF program with typical $R_p \approx 6.0$, $R_{wp} \approx 6.0$, and $\chi^2 \approx 1.0$ X-ray Laue diffraction was used to confirm the quality of the crystal [inset of Fig. 1(a)]. The dc magnetic-susceptibility measurements were made with a Quantum Design superconducting interference device magnetometer. The specific heat measurements were performed on a Physical Property Measurement System (Quantum Design). For both the magnetic and specific heat measurements on SC, the applied field is along the [110] axis. The thermal conductivity $\kappa(T)$ was measured on SC with a steady-state heat-flow technique.

III. RESULTS

The room-temperature XRD pattern of SC shows a single phase with a cubic, $Fd\bar{3}m$, structure. The lattice parameter is a=8.5063(2) Å [Fig. 1(a)]. Low-temperature XRD experiments were completed to investigate the structural transition in single crystal MnV_2O_4. At low temperatures, the structure changes to tetragonal $I4_1/amd$ symmetry (Figs. 1 and 2). The detailed measurements around the transition (1 K/step) shows that the transition occurs at 52 K, which is shown by the splitting of the cubic (311) Bragg peak, (Fig. 3). Moreover, within a range of temperature between 52 and 46 K, there is evidence for the coexistence of the high-temperature cubic and low-temperature tetragonal phases. Below 52 K, the (333) peak becomes broad due to the coexistence of these two phases, and the peak can be fitted to three Lorentzians (Fig. 4). Among these three peaks, the two peaks with lowest and highest degrees are due to the splitting of the (333) peak into the (321) and (105) Bragg peaks in the tetragonal phase. The central one is the remaining (333) peak belonging to the cubic phase and its intensity decreases with decreasing temperature and disappears at 46 K. The integrated area of the (333) and (321) Bragg peaks was used as a measure of the volume fraction of each phase [Fig. 2(c)]. Within the region of 52–46 K, the total integrated area of the two peaks was constant. The lattice parameters calculated by the FULLPROF program are shown in Fig. 2(a). Between 52 and 46 K, the XRD data could not be fitted with a single $I4_1/amd$ phase due to the broadening of the selected Bragg peaks. The low-temperature data here clearly show that the structural transition occurs at 52 K with phase separation, which indicates that the transition is first order. Another noteworthy structural feature is that if the volume of the tetragonal phase is calculated as $(\sqrt{2}a_t)^2 c_t$, then the sample shows a negative thermal expansion in a temperature range of 10–46 K. This demonstrates the strong magnetoelastic coupling in the ordered phase.

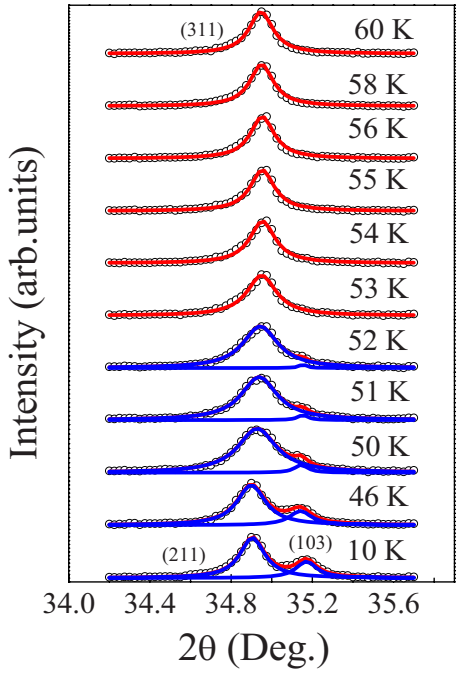

FIG. 3. (Color online) XRD scans of the (311) peak at different temperatures for SC. Circles are experimental data; red and blue lines are Lorentzian fits. Note the structural transition occurring at 52 K.

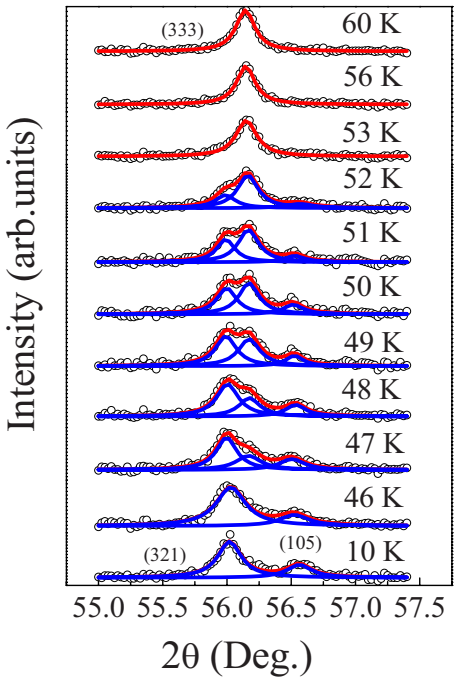

FIG. 4. (Color online) XRD scans of the (333) peak at different temperatures for SC. Circles are experimental data; red and blue lines are Lorentzian fits. Note the region of phase coexistence from 52 to 46 K.

The room-temperature XRD pattern of PC also shows a single phase with a cubic, $Fd\bar{3}m$, structure. Compared to SC, PC has a larger lattice constant with $a=8.5210(2)$ Å (Table I). The temperature dependencies of the (311) (Fig. 5) and (333) (Fig. 6) peaks of PC are similar to those of SC. However, for PC, the structural transition occurs at 55 K and its phase coexistence region is 55–51 K.

The susceptibility of SC sharply increases around 60 K due to the ferrimagnetic transition. Below 60 K, the data show two peaks at 56 and 52 K [Fig. 7(a)]. This is different from the previous reported data on single crystals,[10] which just show one peak at 57 K. Below 50 K, there is a difference in the field-cooled (FC) and zero-field-cooled data (ZFC), which is due to a spin-glass-like ground state developing at low temperatures. NMR measurements and ac susceptibility have recently demonstrated this in a separate publication.[12] The specific heat data of SC [Fig. 7(b)] here also show two anomalies at the same temperatures, which indicate that there are two phase transitions.

For the PC sample, both susceptibility and specific heat (Fig. 7) just show one transition at 55 K. The absolute value of the specific heat of PC is much smaller than that of SC, which may be due to the grain boundary effect from PC.

TABLE I. Room-temperature crystallographic parameters and selected bond lengths for single crystal (SC) [$a=8.5063(2)$ Å] and polycrystalline (PC) [$a=8.5210(2)$ Å] MnV_2O_4.

Sample	Atom	x	y	z	B (Å^2)
SC	Mn	0.125	0.125	0.125	1.50(4)
	V	0.5	0.5	0.5	1.90(7)
	O	0.2659(2)	0.2659(2)	0.2659(2)	2.30(7)
	Mn-O	2.0752(2) (Å)			
	V-O	2.0009(2) (Å)			
PC	Mn	0.125	0.125	0.125	2.00(4)
	V	0.5	0.5	0.5	2.10(5)
	O	0.2656(2)	0.2656(2)	0.2656(2)	2.30(7)
	Mn-O	2.0751(2) (Å)			
	V-O	2.0062(2) (Å)			

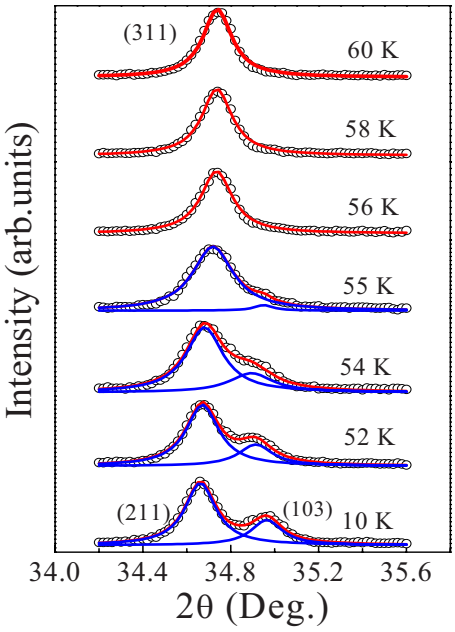

FIG. 5. (Color online) XRD scans of the (311) peak at different temperatures for PC. Circles are experimental data; red and blue lines are Lorentzian fits. Note the structural transition occurring at 55 K.

IV. DISCUSSION

The reported neutron scattering experiments on polycrystalline MnV_2O_4 have revealed that the sample is tetragonal up to 53 K with a triangular ferrimagnetic moment configuration; between 53 K $< T <$ 56 K, it changes to a collinear

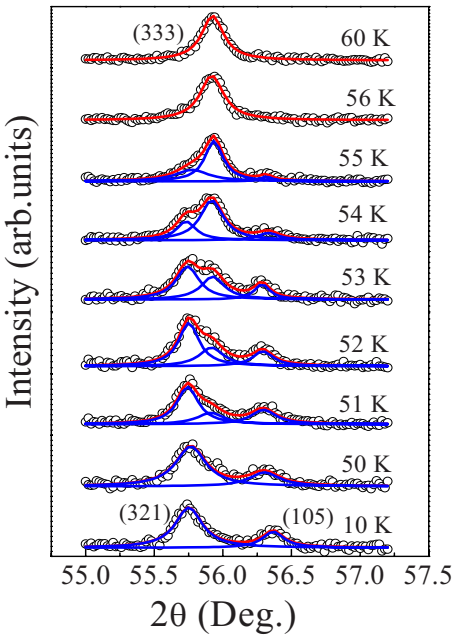

FIG. 6. (Color online) XRD scans of the (333) peak at different temperatures for PC. Circles are experimental data; red and blue lines are Lorentzian fits. Note the region of phase coexistence from 55 to 51 K.

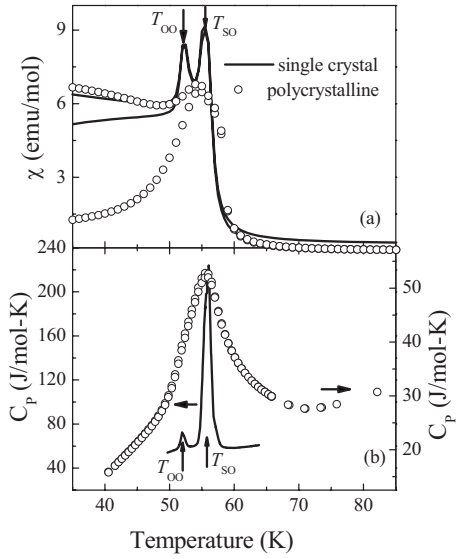

FIG. 7. Temperature dependencies of the (a) dc susceptibility and (b) specific heat of MnV_2O_4. The solid lines represent the SC data and the dots represent the PC data. In (a), the upper curve is the field-cooled (FC) data; the lower curve is the zero-field-cooled data (ZFC).

Néel configuration.[9] These results are consistent with the two phase transitions observed here on the SC sample. Moreover, the structural change at 52 K with the c axis shorter than the a,b axes in the tetragonal phase is similar to the reported data,[10] although the reported structural transition occurs at the same time as the magnetic transition at 57 K. This structural distortion is the same as that of ZnV_2O_4, which stabilizes an "antiferro-orbital" ordering with the yz and the zx orbitals that are alternately occupied along the c axis by splitting the triply degenerate t_{2g} orbitals of V^{3+} ions into a lower energy xy orbital and higher energy yz and zx orbitals.

However, the PC data show just one transition at 55 K. It is noteworthy that at room temperature, the PC sample has a larger lattice constant. By calculating the bond length, it is found that the Mn-O bond length does not change appreciably between the SC and PC samples; however, the PC sample has a larger V–O bond length (Table I), which indicates a vanadium valence change. The bond valence sum is performed based on the structural data in Table I; the result shows that for the SC sample, the vanadium valence is +2.99(1), and for the PC sample, it is +2.95(1). It is clear that the PC sample is nonstoichiometric. Here, we cannot tell whether there is oxygen deficiency or vanadium deficiency in the sample. The latter may be more reasonable due to the evaporation of vanadium during the heating. By adding extra V_2O_3 to the starting materials and selecting growth speed, we were able to grow the stoichiometric and high quality single crystal sample. The observation of only one transition for the nonstoichiometic sample shows that the intrinsic properties of MnV_2O_4 are very sensitive to sample's quality.

Our stoichiometric single crystal sample shows that there are two phase transitions in MnV_2O_4, a spin ordering (ferrimagnetic with a collinear Néel configuration) transition at T_{SO}=56 K, and an orbital ordering transition (ferrimagnetic

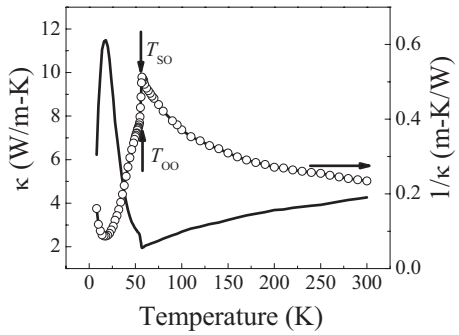

FIG. 8. The thermoconductivity and its inverse for SC MnV_2O_4.

with a triangular configuration) at $T_{OO}=52$ K. The structural transition with phase separation and the sharp peak in the specific heat at 52 K both indicate that the orbital ordering transition is first order. Due to the large value of specific heat at T_{SO}, the absolute value of specific heat at T_{SO} has appreciable error bars. This is an artifact of the relaxation technique. This large value at T_{SO} could be a symbol of a first order transition. However, on the other hand, the ferrimagnetic transition at T_{SO} could also lead a large entropy change to give a large specific heat, which is $S=R\ln(2\times5/2+1)+2R\ln(2\times1+1)=33$ J/mol K. So, the specific heat measurement here is not enough to confirm that the transition at T_{SO} is also first order.

The two transitions in SC are also confirmed by the thermal conductivity measurements. The data (Fig. 8) show a steplike jump at 56 K and a slope change of $1/\kappa$ at 52 K, which indicate changes of scattering mechanism and/or degree of scattering of heat carriers. The steplike jump and slope change take place at temperatures coinciding with T_{SO} and T_{OO}, which can only be explained by the onset of spin and orbital orders. The main features of the thermal conductivity data are as follow. (i) At high temperatures, $\kappa(T)$ shows a positive temperature dependence typical of heat transport in an amorphous solid. This behavior obviously deviates from the $1/T$ law at high temperatures (typical for $T>\theta_D/4$) described by the Debye model for the phonon contribution (κ_{ph}) (Ref. 13); however, it is similar to the thermal conductivity of the other orbital ordering systems, such as the perovskites RVO_3. In RVO_3, $\kappa(T)$ also shows a glassy behavior in an orbitally disordered paramagnetic state.[14] (ii) Spin ordering partially restores the phonon thermal conductivity in the paramagnetic phase; the steplike jump at T_{SO} indicates that the ferrimagnetic phase has a higher thermal conductivity than the paramagnetic phase. (iii) Orbital ordering further restores κ_{ph} and $\kappa(T)$ shows a strong phonon contribution. (iv) The huge phonon peak of the thermal conductivity at low temperatures demonstrates the high quality of our single crystals.

The observation of spin ordering occurring at higher temperatures than that of orbital ordering distinguishes MnV_2O_4 from the other AV_2O_4 cubic spinels (A=Zn, Mg, and Cd) with nonmagnetic ions on A sites, for which the structural transition with orbital ordering occurs at higher temperature than that of the antiferromagnetic ordering. For example, in

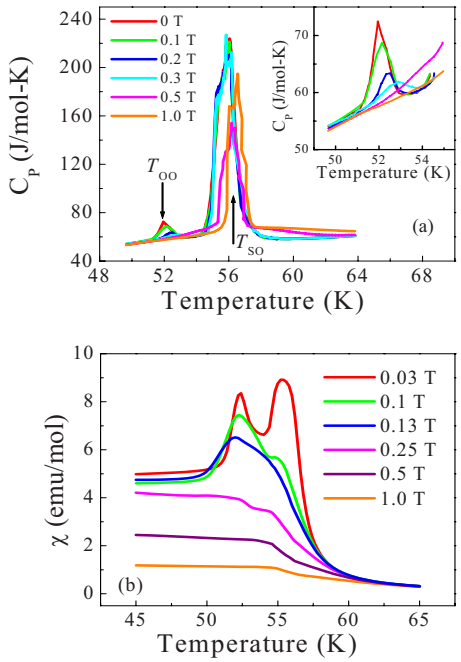

FIG. 9. (Color online) Temperature dependencies of (a) specific heat and (b) ZFC susceptibility around the transitions at different magnetic fields for SC MnV_2O_4. Inset of (a), the enlargement of the peak around T_{OO} at different fields.

ZnV_2O_4 because of geometrical frustration inherent to the B-site network of the spinel lattice, spin ordering ($T_{SO}=40$ K) occurs only after a structural phase transition associated with orbital ordering ($T_{OO}=50$ K). The order of these transitions ($T_{SO}-T_{OO}=4$ K) in MnV_2O_4 is similar to those of the perovskite $LaVO_3$, in which $T_{SO}=143$ K and $T_{OO}=141$ K ($T_{SO}-T_{OO}=2$ K).[15] The theoretical investigation of a spin-orbital model for $LaVO_3$ has shown that the long-range spin ordering endows the orbital system (yz/zx orbitals) with a one dimensional character along the c axis, which produces a strong Jahn-Teller lattice distortion coupled with the orbital ordering.[16] This could be the same reason for why orbital ordering occurs immediately after the spin ordering in MnV_2O_4.

The strong spin-lattice coupling and ferrimagnetism increase the sensitivity of MnV_2O_4 to applied magnetic fields. Figure 9(a) shows the low-temperature specific heat measured under different magnetic fields on SC. Clearly, with the application of small fields ($H<0.5$ T), the intensity of the peak at T_{OO} decreases but T_{OO} increases [Fig. 9(a)]. At higher fields with $H\geqslant0.5$ T, the peak at T_{OO} disappears and the peak at T_{SO} also moves to higher temperatures. The susceptibility data under fields [Fig. 9(b)] show an evolution from a ferrimagnetic behavior at $H=0$ T to a ferromagnetic behavior at higher fields. Moreover, at $H=0.25$ T, there are still traces of two magnetic transitions, and the lower one disappears at $H=0.5$ T, which are in agreement with the specific heat data. Figure 10 shows the field dependencies of T_{SO} and T_{OO}, which are similar to the reported (H,T) phase diagram based on the isofield magnetization measurements.[8] Moreover, our results here show that the system is so sensi-

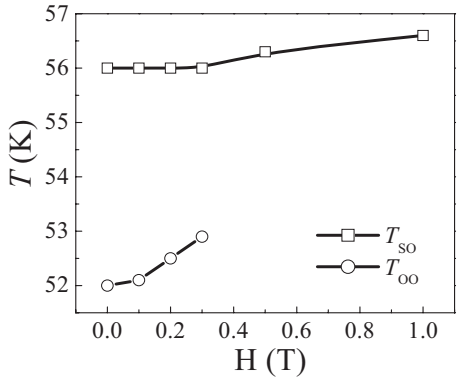

FIG. 10. Field dependencies of T_{SO} and T_{OO}, which are determined by the peak positions of the single crystal specific heat data.

tive to applied fields that the orbital ordering transition disappears with $H \geqslant 0.5$ T. Thus, this transition can be tuned by applied fields, which is rare for t_{2g} electron physics in spinels.

V. CONCLUSION

In summary, there are two transitions in the stoichiometric single crystal MnV_2O_4: a spin ordering transition (T_{SO} =56 K) followed by an orbital ordering transition (T_{OO} =52 K). These transitions are sensitive to the sample's quality. The nonstoichiometic polycrystalline sample just shows one transition at 55 K. The tuning of this system with an applied magnetic field is yet another example of the rich physics offered by geometrically frustrated materials.

ACKNOWLEDGMENTS

This work utilized facilities supported in part by the NSF under Agreement No. DMR-0084173. A portion of this work was made possible by the NHMFL In-House Research Program, the Schuller Program, the EIEG program, and the State of Florida. We acknowledge J. S. Zhou at University of Texas at Austin for the thermal conductivity measurement.

*cwiebe@magnet.fsu.edu

[1] A. P. Ramirez, in *Handbook on Magnetic Materials*, edited by K. J. H. Busch (Elsevier, Amsterdam, 2001), Vol. 13, p. 423.
[2] S. H. Lee, D. Louca, H. Ueda, S. Park, T. J. Sato, M. Isobe, Y. Ueda, S. Rosenkranz, P. Zschack, J. Íñiguez, Y. Qiu, and R. Osborn, Phys. Rev. Lett. **93**, 156407 (2004).
[3] H. Mamiya, M. Onoda, T. Furubayashi, J. Tang, and I. Nakatani, J. Appl. Phys. **81**, 5289 (1997).
[4] N. Nishiguchi and M. Onoda, J. Phys.: Condens. Matter **14**, L551 (2002).
[5] D. I. Khomskii and T. Mizokawa, Phys. Rev. Lett. **94**, 156402 (2005).
[6] O. Tchernyshyov, Phys. Rev. Lett. **93**, 157206 (2004).
[7] M. B. Salamon and M. Jaime, Rev. Mod. Phys. **73**, 583 (2001).
[8] R. Plumier and M. Sougi, Physica B **155**, 315 (1989).
[9] R. Plumier and M. Sougi, Solid State Commun. **64**, 53 (1987).
[10] T. Suzuki, M. Katsumura, K. Taniguchi, T. Arima, and T. Katsufuji, Phys. Rev. Lett. **98**, 127203 (2007).
[11] K. Adachi, T. Suzuki, K. Kato, K. Osaka, M. Takata, and T. Katsufuji, Phys. Rev. Lett. **95**, 197202 (2005).
[12] S. H. Baek, K. Y. Choi, A. P. Reyes, P. L. Kuhns, V. Ramanchandran, N. J. Curro, N. S. Dalal, H. D. Zhou, and C. R. Wiebe, arXiv:0707.0018v1 (unpublished).
[13] R. Berman, *Thermal Conduction in Solids* (Clarendon, Oxford, 1976).
[14] J. Q. Yan, J. S. Zhou, and J. B. Goodenough, Phys. Rev. Lett. **93**, 235901 (2004).
[15] S. Miyasaka, Y. Okimoto, M. Iwama, and Y. Tokura, Phys. Rev. B **68**, 100406(R) (2003).
[16] Y. Motome, H. Seo, Z. Fang, and N. Nagaosa, Phys. Rev. Lett. **90**, 146602 (2003).